Neuron, Vol. 15, 1337–1347, December, 1995, Copyright © 1995 by Cell Press

Hypomyelination Alters K^+ Channel Expression in Mouse Mutants *shiverer* and *Trembler*

Hao Wang,*†‡ Margaret L. Allen,†‡ John J. Grigg,†‡ Jeffrey L. Noebels,§ and Bruce L Tempel*†‡‖
*Department of Otolaryngology–Head and Neck Surgery
†Department of Pharmacology
University of Washington School of Medicine
Seattle, Washington 98195
‡Geriatric Research, Education, and Clinical Center
Veterans Affairs Medical Center
Seattle, Washington 98108
§Developmental Neurogenetics Laboratory
Section of Neurophysiology
Department of Neurology
Baylor College of Medicine
Houston, Texas 77030

Summary

Voltage-gated K+ channels are localized to juxtaparanodal regions of myelinated axons. To begin to understand the role of normal compact myelin in this localization, we examined mKv1.1 and mKv1.2 expression in the dysmyelinating mouse mutants *shiverer* and *Trembler*. In neonatal wild-type and *shiverer* mice, the focal localization of both proteins in axon fiber tracts is similar, suggesting that cues other than mature myelin can direct initial K+ channel localization in *shiverer* mutants. In contrast, K+ channel localization is altered in hypomyelinated axonal fiber tracts of adult mutants, suggesting that abnormal myelination leads to channel redistribution. In *shiverer* adult, K+ channel expression is up-regulated in both axons and glia, as revealed by immunocytochemistry, RNase protection, and in situ hybridization studies. This up-regulation of K+ channels in hypomyelinated axon tracts may reflect a compensatory reorganization of ionic currents, allowing impulse conduction to occur in these dysmyelinating mouse mutants.

Introduction

Electrophysiological studies have identified a variety of voltage-gated K^+ currents in mammalian myelinated axons, where they are presumed to play a role in repolarizing the axons after an action potential (Waxman and Ritchie, 1985; Black et al., 1991; Hille, 1992). K^+ currents are found to be differentially distributed along myelinated axons. Slowly activating voltage-gated K^+ currents are recorded in the axonal membrane at the node of Ranvier, whereas rapidly activating, 4-aminopyridine (4-AP)–sensitive K^+ currents are recorded in the paranodal and internodal regions of acutely demyelinated axons (Chiu et al., 1979; Brismar, 1980; Chiu and Ritchie, 1981; Röper and Schwarz, 1989). Two voltage-gated K^+ channel proteins, mKv1.1 and mKv1.2, may contribute to these K^+ currents, since both have been shown by immunocytochemistry at the electron microscopic level to be highly concentrated at the juxtaparanodal region of myelinated axons (Wang et al., 1993, 1994; Mi et al., 1995).

In comparison to acutely demyelinated axons, chronically dysmyelinated axons show changes in the density and distribution of ionic currents (Bostock et al., 1981; Schwarz et al., 1991). Neither the mechanism(s) nor the molecular identities of the channels involved in these changes are known. In this report, we use immunological and molecular probes specific to mKv1.1 and mKv1.2 to ask, at the molecular level, whether genetic lesions causing chronic dysmyelination result in a spatial reorganization of specific K^+ channels normally expressed in myelinated axon tracts, and whether this reorganization is accompanied by a change in K^+ channel gene expression.

Two mouse mutants, *shiverer* (*shi*) and *Trembler* (*Tr*), provide genetic models to study the effects of chronic dysmyelination. *shi* mice inherit a deletion of 5 exons in the myelin basic protein (MBP) gene (Roach et al., 1985; Molineaux et al., 1986). Homozygous *shi* mice show severe hypomyelination in the CNS and slight hypomyelination in the PNS (Bird et al., 1978; Privat et al., 1979; Rosenbluth, 1980a, 1980b). Myelin sheathes from the *shi* CNS are thin or absent from many large-caliber axons. Where myelin does occur, it is reduced in amount and variable in compactness. Moreover, lamellae frequently do not completely encircle the axons but terminate as loop-like structures within or around the axonal circumference. Axoglial junctions characteristic of the type found in paranodal regions are present in greater than normal numbers and occur in aberrant locations. In spite of these lesions, *shi* mice survive to adulthood, suggesting that nerve conduction is retained. In *shi* mutants, Na^+ channels are elevated in large-caliber myelinated fiber tracts (Noebels et al., 1991; Westenbroek et al., 1992). In *Tr* mice, a substitution of glycine by aspartic acid in the peripheral myelin protein (PMP22) causes the autosomal dominant trembling phenotype (Suter et al., 1992). *Tr* mutants have normal central myelin but severe hypomyelination of peripheral axons. To our knowledge, ion channel expression has not been studied previously in *Tr* mice.

Results

K^+ Channel Distribution Is Altered in CNS Fiber Tracts of *shiverer* Mice

Immunocytochemistry with antibodies to mKv1.1 (α-Kv1.1) and mKv1.2 (α-Kv1.2) showed that the distribution of both proteins was significantly altered and elevated in *shi* hypomyelinated fiber tracts, including cerebellar (Figures 1a and 1b; mKv1.2 is shown) and subcortical white matter, internal capsule, corpus callosum (Figures 1e–1h; mKv1.1

‖Present address: The V. M. Bloedel Hearing Research Center, Box 357923, University of Washington School of Medicine, Seattle, Washington 98195-7923.

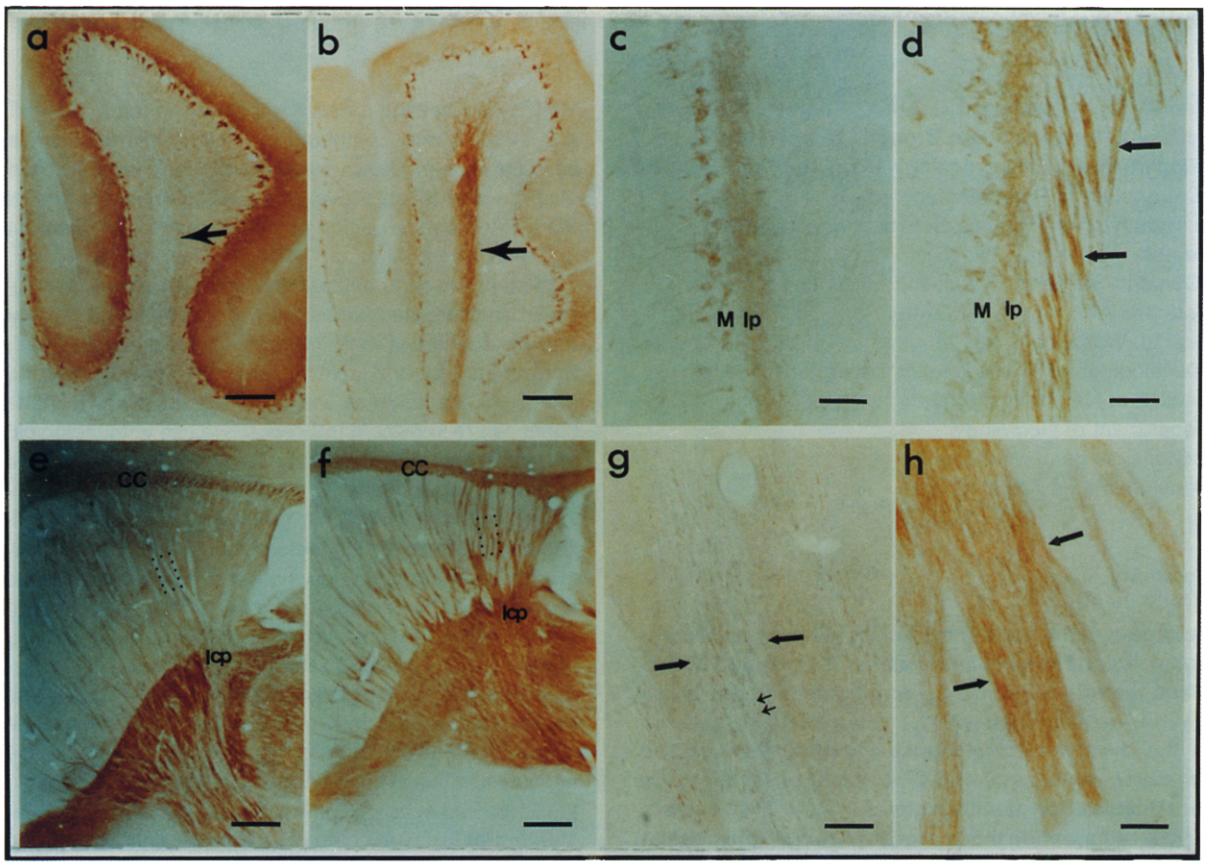

Figure 1. Indirect Peroxidase Staining of mKv1.1 and mKv1.2 Proteins in Different Regions of Wild-Type and *shi* Mouse Brains

(a and b) α-Kv1.2 staining in wild-type (a) and *shi* (b) cerebellum. A picture of slightly longer exposure of a wild-type section was chosen to avoid underestimation of the difference in the fiber tract regions as compared with that of the *shi* mouse. Striking differences in staining are seen in the *shi* corpus medullare (arrow).

(c and d) α-Kv1.2 staining in wild-type (c) and *shi* (d) olfactory bulb. Note the change in staining pattern in the axon tracts (arrows) likely to arise from tufted (not shown) and mitral (M) cells. lp, inner plexiform layer.

(e and f) α-Kv1.1 staining in the corpus callosum (CC), internal capsule (lcp), and corticofugal fiber tracts (boxed) in wild-type (e) and *shi* (f) mice. All mutant fiber tracts show increased staining.

(g and h) Higher magnification of corticofugal fiber staining in regions similar to those boxed in (e) and (f). The border of a major fiber bundle is indicated by large arrows. The pattern of staining within the bundle changes from paired punctate staining (g, small arrows) to more fibrous staining in the *shi* mouse (h).

Bars, 200 μm (a, b, e, and f), 40 μm (c and d), 20 μm (g and h).

is shown), anterior commissure (data not shown), and brain stem (Figures 2a and 2b; mKv1.1). In each of these fiber tracts, the paired punctate staining pattern characteristic of juxtaparanodally localized mKv1.1 and mKv1.2 in wild-type mice changed to intense, diffuse staining in *shi* mice (Figures 1g, 1h, 2a, and 2b). Similar staining patterns were observed with *shi* mice in two different genetic backgrounds, C57BL/6J (Figure 1) and C3HeB (Figures 2–8). While K^+ channel staining increases in *shi* axon tracts, no significant change was observed in the channel-specific distribution or amount of staining in neuronal somata of *shi* brain as compared with wild-type brain (Figure 1; also see Wang et al., 1994). These data suggest that the cell-specific expression patterns of K^+ channels are retained in *shi* mutants, although channel localization is altered in dysmyelinated fiber tracts.

K^+ Channel Redistribution in Fiber Tracts of *Tr* Mice

To test whether the change of staining in hypomyelinated fibers is due specifically to the lack of MBP, we examined the K^+ channel distribution in peripheral nerve fibers of *Tr* mice. In contrast to the dramatic change of staining pattern in the *shi* mice (compare Figures 2a and 2b), no significant change was observed in the α-Kv1.1 and α-Kv1.2 staining pattern in *Tr* brain stem fiber tracts (Figure 2c; mKv1.1). In the peripheral sciatic nerve, myelinated axons in *shi* mice showed only a slight increase in internodal staining and occasional elongated juxtaparanodal profiles (compare Figures 2d and 2e), consistent with reports of minor morphological abnormalities in *shi* peripheral myelin (Rosenbluth, 1980a). In the hypomyelinated *Tr* sciatic nerve, more diffuse staining was seen for either channel than in *shi* sciatic nerve (Figure 2f; mKv1.1). In each mutant strain,

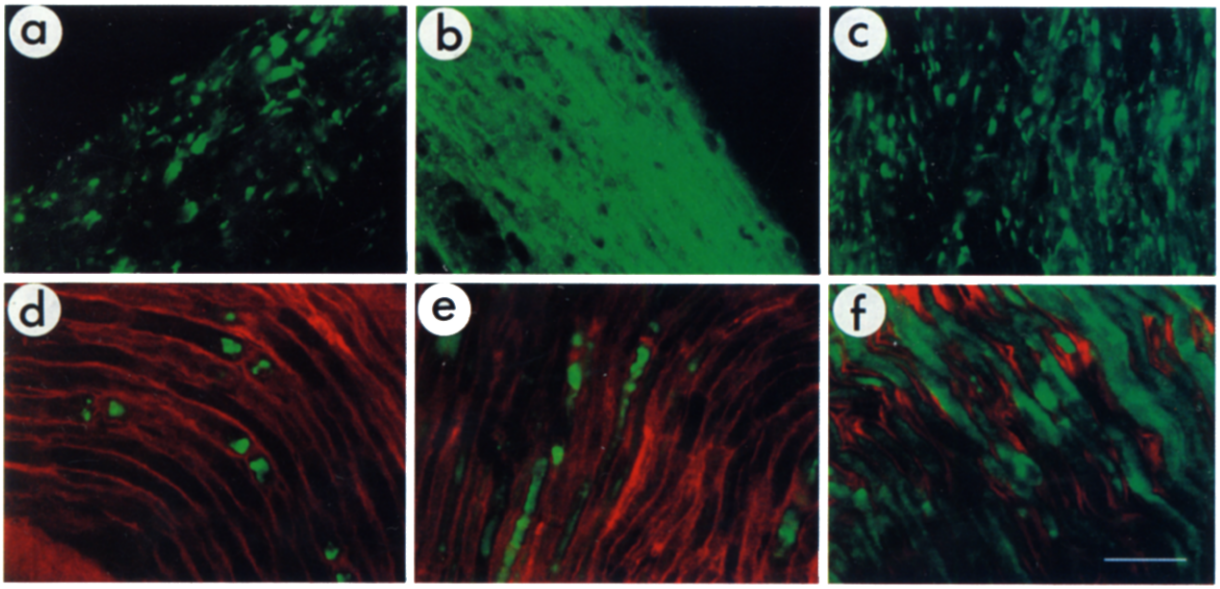

Figure 2. Fluorescence Immunocytochemistry of mKv1.1 in Ventral Fiber Tracts of the Brain Stem and Sciatic Nerve of Wild-Type and *shi* Mice

All sections were stained in parallel, and images were collected using the same aperture and gain in the confocal microscope in order to compare the relative levels of staining.

(a–c) α-Kv1.1 staining of brain stem in +/+ (a), *shi*/*shi* (b), and *Tr*/+ (c) mice. The *shi* fiber tracts show a diffuse staining pattern.

(d–f) Double staining with α-Kv1.1 (green) and α-CNP (red) in sciatic nerve of +/+(d), *shi*/*shi* (e), and *Tr*/+ (f) mice. Note the occasional mildly elongated internodal staining for mKv1.1 in *shi* axons in contrast to the more diffuse distribution in *Tr* sciatic nerve. Bar, 10 μm.

the major changes in K^+ channel redistribution were confined to regions of hypomyelination. These results suggest that normal myelination, rather than the specific absence of either MBP or PMP22, contributes to the juxtaparanodal localization of mKv1.1 and mKv1.2 proteins seen in normal animals.

Cellular Localization of K^+ Channels

To determine whether the aberrant increase in staining within the mutant fiber tracts originates in axons or glia, we examined the localization of K^+ channels in *shi* and *Tr* fiber tracts, both by confocal microscopy and by three-dimensional fluorescence imaging using a Deltavision Wide-Field Deconvolution microscope. Brain stem sections were double stained with α-Kv1.1 and an antibody specific to the 2′,3′-cyclic nucleotide 3′-phosphodiesterase (CNP) (Figure 3). CNP staining identifies both cytoplasm and myelin membranes of oligodendrocytes and Schwann cells. CNP can be used as a glial marker in both *shi* and *Tr* mice because its expression is unaffected in *shi* adult and reduced to about 65% of normal in *Tr* PNS (reviewed by Sprinkle, 1989). In wild-type mice at high magnification using a confocal microscope, the intense α-mKv1.1 staining did not overlap with the glial α-CNP staining (compare Figures 3a, 3b, and 3c). In sections from *shi* mice, α-Kv1.1 staining occurred at distinct levels of intensity (Figure 3e). The faint, more diffuse α-mKv1.1 staining was generally higher in *shi* mice than in the wild type (Figure 3e versus Figure 3b, boxed regions). This faint α-mKv1.1 staining colocalized with α-CNP staining, giving rise to a yellowish tint in the superimposed image (Figure 3f, boxed regions).

In contrast to the faint α-mKv1.1 staining in regions of glia, the intense staining seen in Figure 3 appears to be associated with axons. To confirm that K^+ channel proteins are redistributed in axons of hypomyelinated fiber tracts in the mutants, we used a Deltavision SA3 Wide-Field Deconvolution microscope to obtain high magnification and high resolution images (Figure 4). We studied the localization of K^+ channels in serial 0.2 μm optical sections taken from 20 μm histochemical sections of *Tr* sciatic nerve and *shi* brain stem and spinal cord. In *Tr* mice, the K^+ channel staining is associated with axolemma and within axons in several optical sections progressing through a section of sciatic nerve (Figure 4). Note the extensive longitudinal distribution of K^+ channel staining along the axon. Similar axonal K^+ channel redistribution is also observed in the brain stem and spinal cord sections of *shi* mice (data not shown).

Collectively, these results demonstrate that K^+ channel distribution and expression are altered in both axons and glia of hypomyelinated fiber tracts.

K^+ Channel RNA Increases in Both Neurons and Glia of *shiverer* Mice

To determine whether K^+ channel redistribution reflects up-regulation of gene expression, RNase protection assays were performed, comparing the steady-state levels of mKv1.1 and mKv1.2 RNA in the *shi* brain to those in the wild-type brain. For each experiment, total RNA was isolated from gross dissection of separate brain regions, pooled from three *shi* and three wild-type mice. The relative ratios of mKv1.1 or mKv1.2 to that of 18S ribosomal

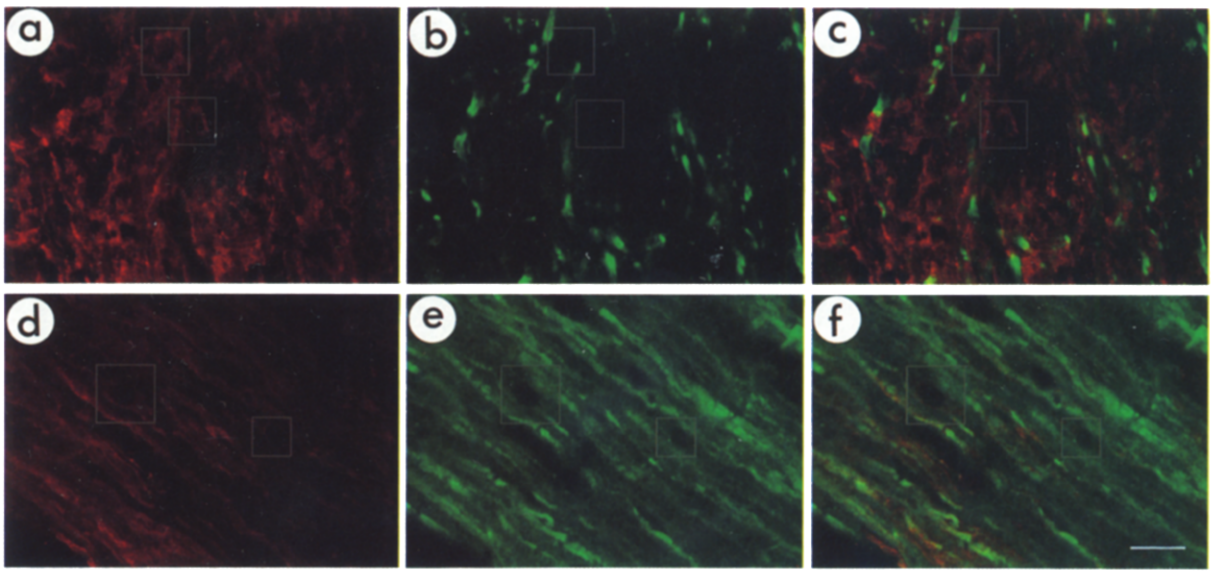

Figure 3. Double Fluorescence Immunocytochemistry of mKv1.1 and α-CNP in Ventral Tracts of Brain Stem

(a–c) Wild-type staining with α-CNP (a; red) and α-Kv1.1 (b; green), and images from (a) and (b) superimposed (c). No α-Kv1.1 staining is seen in the region of glia (boxed regions).

(d–f) *shi* mouse stained with α-CNP (d) and α-Kv1.1 (e), and images from (d) and (e) superimposed (f). Note that two levels of intensity are seen in (e): intense staining in axons and faint staining overlying glia (boxed regions).

Bar, 5 μm.

RNA were calculated by PhosphoImager quantitation of protected fragments. Three independent experiments were performed. Consistent 2- to 4-fold increases were observed in each experiment for each K^+ channel RNA in three separate brain regions (Figure 5; Table 1).

We performed in situ hybridization studies on brains from both *shi* and wild-type animals in order to resolve at the cellular level the source of these changes in expression. Striking increases were observed in autoradiographic signal density for mKv1.1 and mKv1.2 RNA in fiber tracts (Figure 6). In particular, a significant increase in mKv1.1 signal was noted in the corpus callosum, anterior commissure, internal capsule, and corpus medullare of *shi* mice (Figures 6a, 6b, 6g, and 6h). Similar, though smaller, increases in mKv1.2 expression were seen in the same fiber tracts (Figures 6c and 6d). No change was observed for mKv3.1 (Figures 6e and 6f). Integrated optical density (IOD) from the autoradiograms in several fiber tracts and neuronal regions was analyzed for the expression level of mKv1.1 and mKv1.2 RNA. The aggregate data show that mKv1.1 RNA increased about 3-fold in *shi* fiber tracts, while mKv1.2 increased about 1.5-fold (Table 2).

Analysis of emulsion-dipped slides showed that increases in both cell number and expression per cell within the hypomyelinated fiber tract contribute to the observed increase in K^+ channel expression by IOD measurement. In each section, we analyzed all the cells in the corpus callosum that were 1 mm from the midline. Counting the number of hematoxylin-stained nuclei revealed a mean 1.5-fold increase in the density of nuclei in *shi* over wild-type mice. The number of silver grains per cell in the corpus callosum in 9 pairs of sections of *shi* and wild-type mice were determined using the MCID system (see Experimental Procedures; Figures 6i and 6j). Binned according to the number of silver grains per cell, a greater percentage of cells with high expression of mKv1.1 was found in *shi* mice. The maximum expression level was also increased from 8 grains/cell in the wild type to 11 grains/cell in *shi* mutant (Figure 6k and 6l). We conclude from these studies that expression levels of both mKv1.1 and mKv1.2 increased in *shi* glial cells. For mKv1.2, the increase may be accounted for by an increase in glial cell number in the fiber tracts. For mKv1.1, expression increased on a per cell basis.

To evaluate changes in K^+ channel RNA levels in neurons, the expression of mKv1.1 and mKv1.2 was analyzed in neurons of the deep cerebellar nuclei at two different parasagittal planes, medial and lateral. These nuclei were chosen because individual cells in the nuclei are well isolated and easily distinguishable and because the expression of mKv1.1 and mKv1.2 is relatively high and homogenous (Figure 7). These bilateral symmetric nuclei receive input from Purkinje cells and project to other brain regions along myelinated brain stem fiber tracts. Although the relative increases varied between subnuclei, an average >1.5-fold increase in the number of silver grains was found for both mKv1.1 and mKv1.2 (Figure 7e). These data corroborate our observations of increased K^+ channel proteins in *shi* axons by immunocytochemistry.

Changes in Axon K^+ Channel Distribution during Development

To determine whether normal compact myelin is required for channel localization in axon fiber tracts during early postnatal development, cervical and lumbar regions of wild-type and homozygous *shi* spinal cords were stained

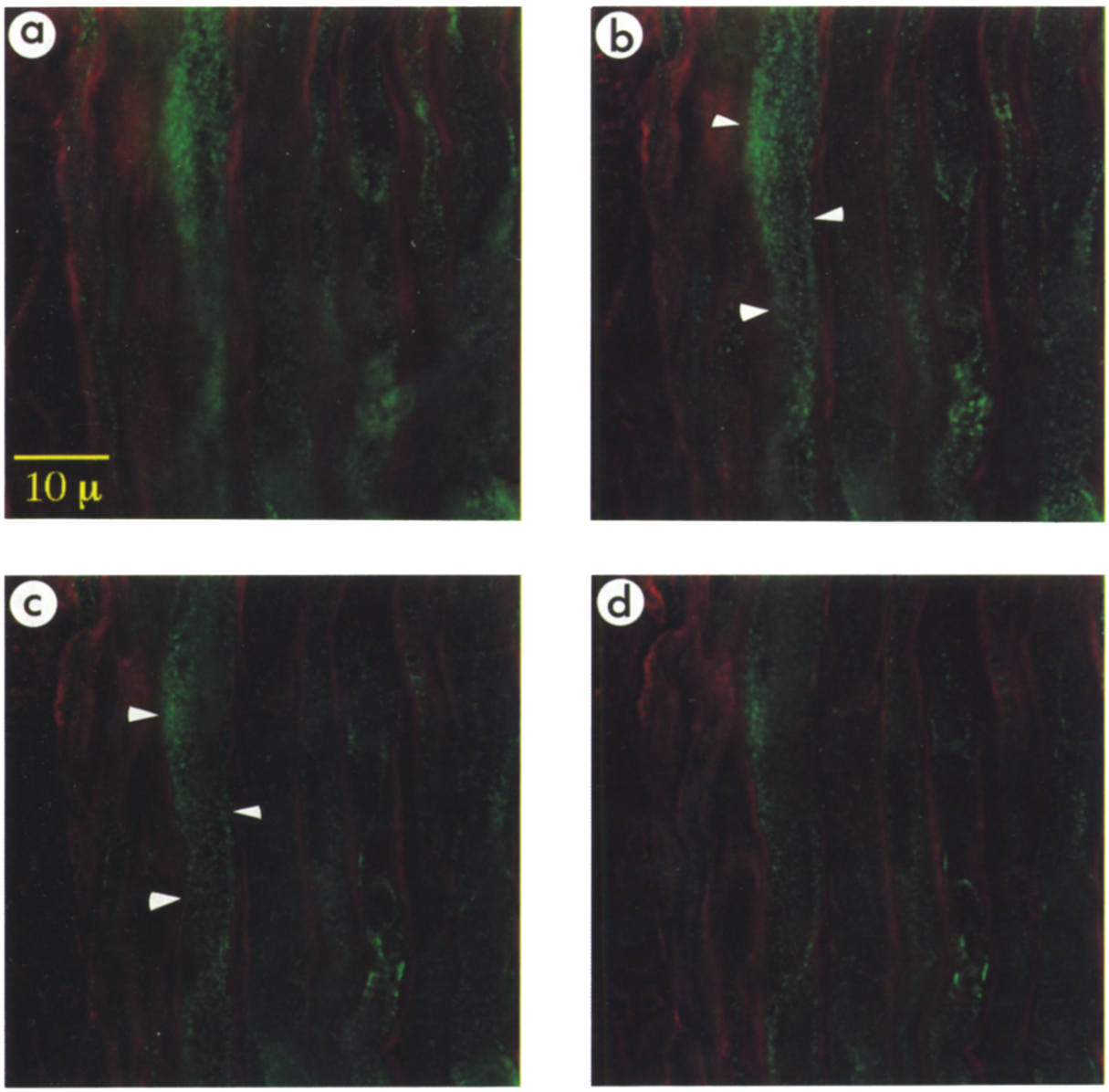

Figure 4. Double Fluorescence Immunocytochemistry of α-mKv1.1 and α-CNP in Sciatic Nerve of *Tr* Mice

Images were obtained using a Deltavision Wide-field Deconvolution microscope and show representative sections selected from a series of 32 optical sections. The thickness of each optical section is 0.2 μm. Sections are 0.4 μm apart from each other. Note the α-mKv1.1 staining within several axons. Arrowheads highlight one axon shown in (b) and (c).

using α-Kv1.1 and α-Kv1.2 at postnatal day 2 (P2) and various ages to adult. Although cell somata were heavily stained by α-Kv1.1, no immunoreactivity was detected in either dorsal or ventral white matter at P2. A similar pattern was observed at P6. At P8, faint paired punctate staining was observed in a few fibers in both genotypes (data not shown). At P13, paired punctate staining was clearly discernible in both wild-type and *shi* spinal cord (Figures 8a and 8b; mKv1.2). At P17, however, clear differences in the level of staining along the axon tracts became apparent between wild-type and *shi* spinal cord (Figures 8c and 8d; mKv1.2). The density of juxtaparanodal profiles continued to increase in wild-type spinal cord through P63 (Figure 8e; mKv1.2), while in the *shi* spinal cord, high levels of more diffuse staining and patches of intense staining were observed (Figure 8f; mKv1.2 is shown). These experiments show that mKv1.1 and mKv1.2 are localized similarly in *shi* and wild-type axon tracts during early postnatal development, even though *shi* mice never develop normal compact myelin.

Discussion

Results from our studies on *shi* and *Tr* mice suggest that hypomyelination alters K+ channel localization and gene expression, independently of the specific genetic lesion that causes dysmyelination. Further support for this conclusion is provided by a similar finding in the *jimpy* mouse,

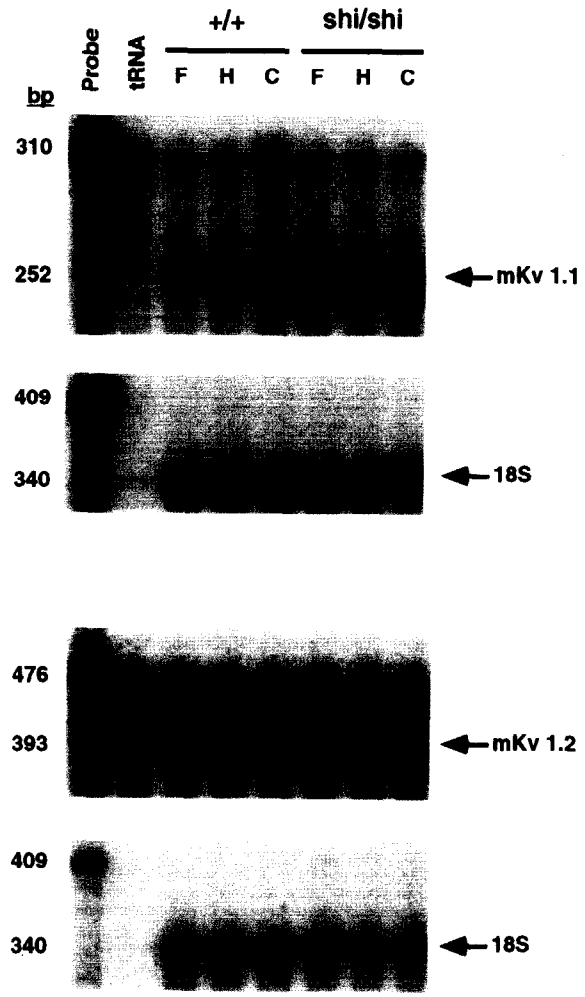

Figure 5. RNase Protection Assay on Total RNA Prepared from Wild-Type and *shi* Homozygous Mouse Brains

For each mouse strain, brains were dissected into the following regions: cerebral hemispheres (F), Pons and medulla (H), and cerebellum (C). In each set of assays that protected one of the K^+ channel mRNAs (mKv1.1 or mKv1.2), loading was monitored by diluting an aliquot of the sample by 10^{-4} and protecting a 340 bp fragment of 18S rRNA.

Table 1. K^+ Channel Gene Expression Measured by RNase Protection

	Wild Type	*shi*	*shi*/Wild Type
mKv1.1			
Forebrain	0.267	0.838	4.0 ± 1.0
Hindbrain	0.406	1.725	3.7 ± 0.8
Cerebellum	0.658	2.086	2.7 ± 0.4
mKv1.2			
Forebrain	0.252	0.346	1.6 ± 0.2
Hindbrain	0.317	0.722	2.1 ± 0.3
Cerebellum	0.280	0.646	2.2 ± 0.3

Values (left two columns) from one K^+ channel expression assay represent ratios determined by dividing the signal intensity of the protected K^+ channel RNA fragment by that determined for 18S in the corresponding lane. In the right column, values from three independent sets of assays (each on a pool of RNA from three brains) are averaged and presented as the ratio of K^+ channel gene expression in *shi*/wild type.

a severe hypomyelinating mutant that has a mutation in the sex-linked proteolipid protein gene. Most of the oligodendrocytes in these mice die and do not generate myelin sheath. Consistent with the role of compact myelin in K^+ channel localization, in hemizygous or homozygous *jimpy* mice, the K^+ channel distribution is dispersed along axon fiber tracts (H. W. and B. L T., unpublished data).

Elevated K^+ Channel Expression in Neurons and Axons

When expressed in Xenopus oocytes or in transformed mammalian cells, both mKv1.1 and mKv1.2 give rise to rapidly activating, voltage-gated K^+ currents that are blocked by relatively low concentrations of 4-AP (Werkman et al., 1992; Bosma et al., 1993; Hopkins et al., 1994). K^+ currents with similar properties are present in axons (Waxman and Ritchie, 1985). Immediately after acute demyelination, action potential conduction is blocked, presumably owing to the abundance of these K^+ channels (previously covered by myelin) relative to the low density of Na^+ channels in the internode (Shrager, 1989). In this situation, decreasing K^+ currents with the K^+ channel blocker 4-AP promote conduction (Bostock et al., 1981; Waxman and Wood, 1984; Targ and Kocsis, 1985), suggesting that the relative strength of K^+ and Na^+ currents is a primary determinant of successful action potential propagation. In clinical trials, patients with multiple sclerosis have shown improvement in their symptoms when treated with 4-AP (Stefoski et al., 1987; Bever, 1994). Blocking the paranodal K^+ channels in demyelinated axons with 4-AP can also lead to repetitive firing following a single impulse (Bowe et al., 1985; Baker et al., 1987). Together, these experiments on dysmyelinated axons suggest that the level of axonal K^+ currents critically influences proper action potential conduction.

We show here by quantitative in situ hybridization that levels of mKv1.1 and mKv1.2 mRNA increase in deep cerebellar nuclei of *shi* mutants. Furthermore, immunocytochemical studies reveal an increase and redistribution of mKv1.1 and mKv1.2 in *shi* axons. In *shi* mice, type II Na^+ channel density has been demonstrated to be increased in axon tracts (Westenbroek et al., 1992). Assuming that at least part of the increase in Na^+ channel expression occurs in axons, the up-regulation of mKv1.1 and mKv1.2 in *shi* mice may provide a more favorable electrophysiological balance between Na^+ and K^+ currents, an adaptive mechanism for impulse conduction. In support of this hypothesis, the sites of elevated expression of K^+ channels are found to coincide with the sites of Na^+ channel increase in many large-caliber fiber tracts.

Elevated K^+ Channel Expression in Glia

Electrophysiological studies have shown that rapidly activating, sustained K^+ currents exist in mature glia, including oligodendrocytes and Schwann cells (Barres, 1991; Chiu, 1991). The molecular identities of the K^+ channels expressed in Schwann cells have recently been investigated. Northern blot analysis of rat sciatic nerve has shown that transcripts for Kv1.1 and Kv1.2 increase from P1 to P15 and then decline modestly (Chiu et al., 1994). Kv1.1 pro-

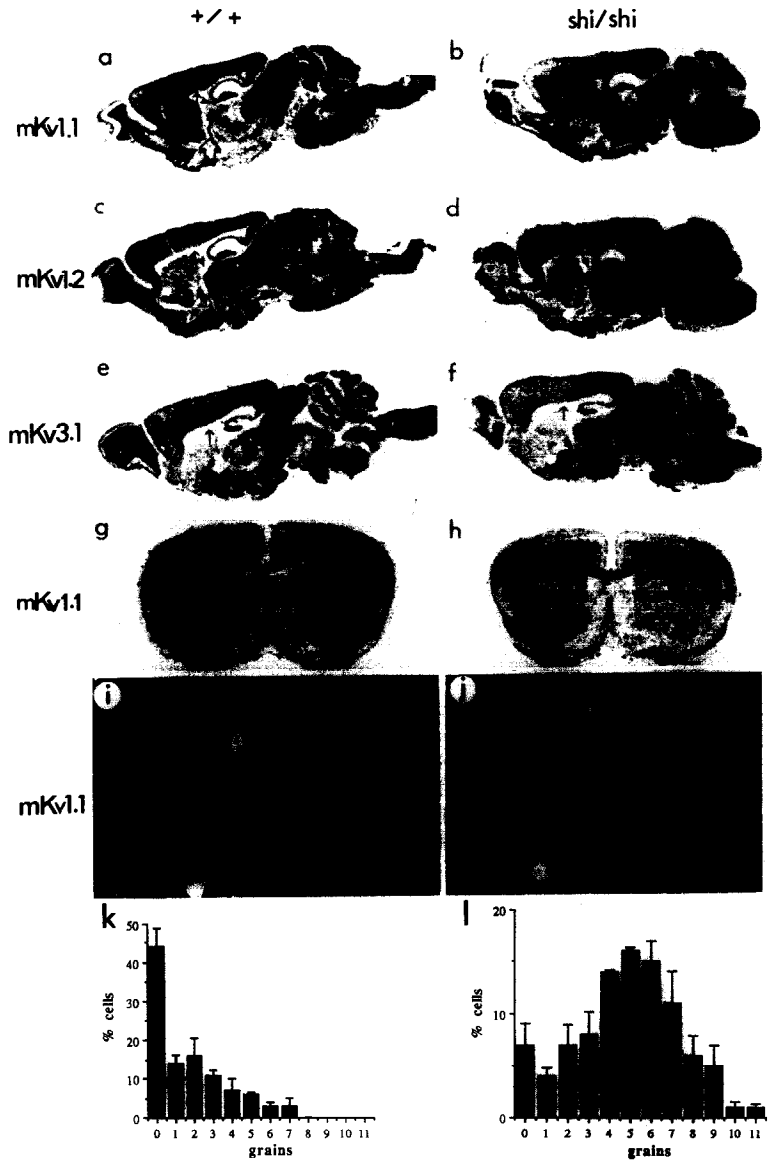

Figure 6. In Situ Hybridization of K+ Channels in Wild-Type and *shi* Brain

(a–h) Photographs from autoradiograms. Parasagittal sections were labeled with mKv1.1 antisense probe (a and b), mKv1.2 antisense probe (c and d), or mKv3.1 antisense probe (e and f). In corpus callosum (arrows) and fornix-fimbria (arrowheads), a clear increase is seen for mKv1.1; a small change is seen for mKv1.2; no change is seen for mKv3.1. Coronal sections (g and h) were labeled with mKv1.1 and show the changes in corpus callosum (arrows).

(i and j) Corpus callosum under dark-field illumination. Notice the bright, clustered silver grains. Arrowheads indicate the margin of the fiber tract. Bar, 100 μm (i and j).

(k and l) Cellular mKv1.1 expression in the corpus callosum. Cells were binned according the number of silver grains in the corpus callosum of wild-type (k) and *shi* (l) mice. Data show averages from 9 sections in three animals of each genotype. Note the greater percentage of cells that have higher expression in the *shi* mouse, as well as the change in the maximum number of silver grains per cell.

tein is detected in the perinuclear, intracellular compartment, while mKv1.5 is present in Schwann cell membrane at the node of Ranvier and in bands that run along the outer surface of the myelin (Mi et al., 1995). To our knowledge, the molecular identities of K+ channels in oligodendrocytes in vivo have not been reported.

Our in situ hybridization and immunocytochemistry data suggest that K+ channel expression is chronically up-regulated in glia of *shi* mice, and that the RNA level of mKv1.1 is increased on a per cell basis. It is possible that in the absence of MBP *shi* glia retain a less differentiated state of channel expression, correlating with their failure to form uniformly compacted myelin (Rosenbluth, 1980b). Alternatively, oligodendrocytes in *shi* mice may be replaced at a higher than normal rate, and mKv1.1 expression may be up-regulated to support glial cell proliferation (Chiu and Wilson, 1989; Wilson and Chiu, 1990). Finally, K+ channels may be up-regulated in glia to support increased K+ transfer and buffering, secondary to increased neuronal activity and K+ efflux in the adjacent axons (Barres, 1991; Chiu, 1991). At present, we cannot distinguish among these or other possibilities.

Table 2. Ratio of K+ Channel mRNA Expression in *shi* and Wild-Type Mice

	mKv1.1	mKv1.2
Corpus callosum	3.90 ± 0.23	1.40 ± 0.02
Fornix-fimbria	3.30 ± 0.11	1.52 ± 0.06
Internal capsule	2.26 ± 0.04	1.43 ± 0.13
Hippocampus	1.09 ± 0.03	1.09 ± 0.04
Cortex	1.09 ± 0.07	1.15 ± 0.08
Olfactory bulb	–	1.14 ± 0.05

Data are ratios of mRNA expression in various brain regions of *shi* mice, determined by in situ hybridization, to that of wild-type mice, measured by IOD readings from in situ hybridization autoradiograms. Values are the average of ratios from 9 pairs of sections from three pairs of animals.

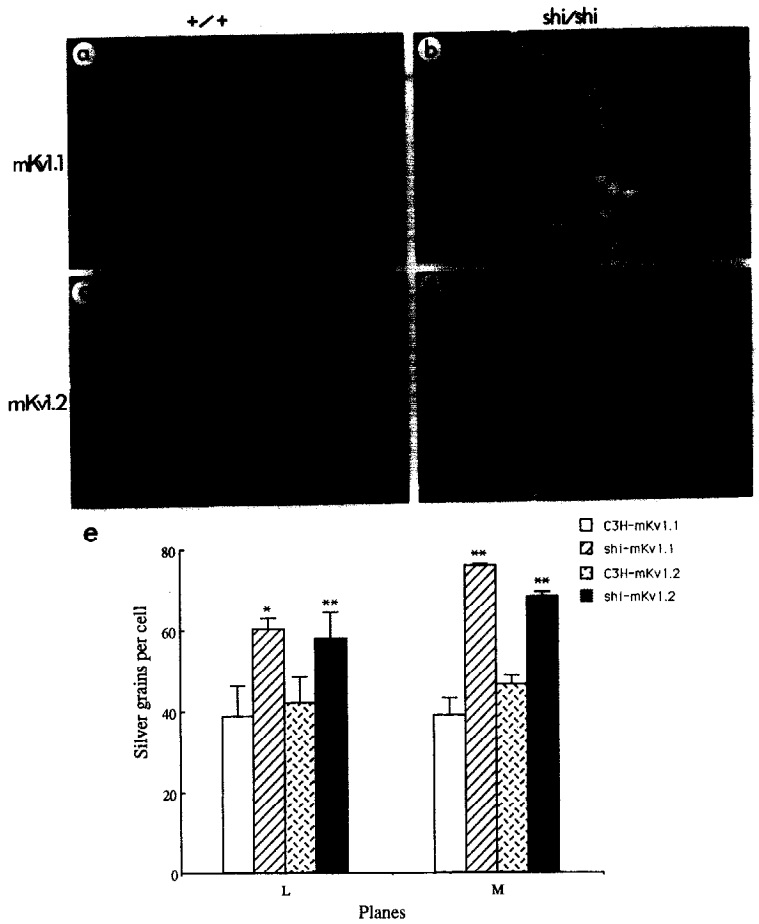

Figure 7. Dark-Field Image of In Situ Hybridization of mKv1.1 and mKv1.2 in Deep Cerebellar Nuclei Shows Increased Level of Neuronal Expression

(a) mKv1.1 in wild-type C3H brain.
(b) mKv1.1 in *shi* brain.
(c) mKv1.2 in wild-type C3H brain.
(d) mKv1.2 in *shi* brain. Bar, 20 μm.
(e) The number of silver grains per cell in two parasagittal planes of the deep cerebellar nuclei, lateral (L) and medial (M). Results are averages of 9 pairs of sections from three groups of animals. The difference between *shi* and wild-type C3H mice is statistically significant by Student's t test at $p = .05$ (*) or $p < .04$ (**).

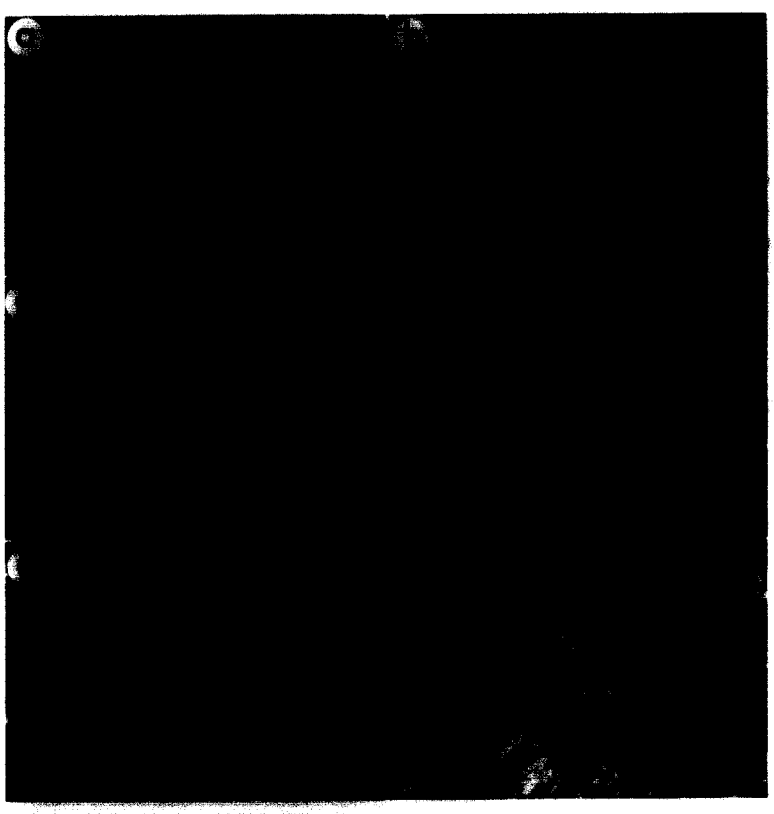

Figure 8. Developmental Changes in the Distribution of mKv1.2 Proteins in Ventral Fiber Tracts of Lumbar Spinal Cord during Development in Wild-Type and *shi* Mice

(a and b) At P13, both wild-type (left) and *shi* (right) mice show paired punctate staining.
(c and d) At P17, the paired punctate staining profiles are increased in wild type (left). The staining is more diffuse in the *shi* mouse (right).
(e and f) In the young adult mouse (63 days), the paired punctate staining is more distinct in wild type, while a more diffuse pattern of staining is seen in *shi* axon fiber tracts.
Bar, 5 μm.

Ion Channel Regulation in Fiber Tracts during Development

In early postnatal mouse spinal cord, scattered myelin-ensheathed axons are visible at P2 in ventral columns of cervical segments, become abundant by P5, and continue to increase in number and diameter through 2 months of age (Choi, 1986). We observed paired, punctate juxtaparanodal K^+ channel profiles in both wild-type and *shi* mutants from P8 through P14. This observation suggests that the signals required for initial localization of K^+ channels are present in *shi* mice, which never develop normal compact myelin. These signals may include axonal membrane specializations that are present in both wild-type and *shi* mice (Wiley-Livigston and Ellisman, 1980; Rosenbluth, 1981; Rosenbluth, 1988). Alternatively, neuron–glia contact may play an important role in K^+ channel localization, as has been demonstrated for clustering of Na^+ channels during remyelination in vivo (Dugandzija-Novakovic et al., 1995).

After P14, mKv1.1 and mKv1.2 protein staining increases and becomes more diffuse in *shi* fiber tracts. This failure to maintain K^+ channel localization in *shi* adults may be due to altered structural or trophic interactions between glia and neurons. Alternatively, increases in Na^+ channel number and maturity observed during postnatal weeks 2–3 in normal rat brain development (Gordon et al., 1987; Scheinman et al., 1989) may cause electrical hyperactivity in hypomyelinated axons, inducing K^+ channel expression. Reciprocally, demyelination studies in adults argue that relatively overabundant K^+ channels may suppress electrogenesis (Bostock et al., 1981; Waxman and Wood, 1984; Targ and Kocsis, 1985), perhaps inducing Na^+ channel up-regulation. Further studies are needed to determine the relative contributions of glia and intrinsic neuronal regulation of ion channels in response to dysmyelination.

In summary, changes in glial and neuronal K^+ channel expression observed in *shi* and *Tr* mice may provide information relevant to diseases of dysmyelination. Identical point mutations are found in the PMP22 gene in human patients with the peripheral neuropathy, Charcot–Marie–Tooth type 1A, and in one *Tr* allele, Tr^J (Valentijn et al., 1992). In addition, *shi* mutants provide a model for some of the effects of multiple sclerosis. Increases in Na^+ channel expression occur in *shi* CNS fiber tracts (Noebels et al., 1991; Westenbroek et al., 1992); similar increases in Na^+ channel expression are observed in patients with multiple sclerosis at sites of lesion (Moll et al., 1991). Although the molecular mechanisms that establish and maintain the juxtaparanodal localization of K^+ channels in myelinated axons are not known, changes in ion channel regulation similar to those observed in *shi* and *Tr* mutants may occur in human diseases where normal myelination is disrupted.

Experimental Procedures

Mice

Mutant C57BL/6J-*shi*/*shi* mice were maintained at the Baylor College of Medicine. Breeding pairs of C3HeB-+/*shi* and C57BL/6J-+/*Tr* mice were obtained from Jackson Laboratory and maintained at the Seattle Verteran's Administration medical center by mating confirmed heterozygotes. *shi* homozygotes and *Tr* heterozygotes were identified by their phenotypes. For developmental studies, *shi* homozygotes were obtained by mating homozygotes.

Immunocytochemistry

Antibodies recognizing mKv1.1 and mKv1.2, α-Kv1.1 and α-Kv1.2, respectively, were purified using an immunoaffinity–immunoabsorption procedure as described (Wang et al., 1993). For peroxidase-based staining, frozen sections (35 μm) from three wild-type (C57BL/6J-+/+) and three *shi* (C57BL/6J-*shi*/*shi*) mice were cut on a sliding microtome. Free-floating sections were processed for immunocytochemistry using the indirect peroxidase anti-peroxidase technique (Sternberger, 1979) with slight modifications as described (Wang et al., 1994).

For fluorescence staining, three C3HeB-+/+ and three C3HeB-*shi*/*shi* mice or three C57BL/6J-+/+ and three C57BL/6J-*Tr*/+ mice were analyzed for each experiment; 20 μm cryostat sections were used. Fixation and immunocytochemistry were done according to Sternberger (1979) with modifications as described (Wang et al., 1993). Double staining with either α-Kv1.1 or α-Kv1.2 in combination with α-CNP (Boehringer) was performed by coincubation with α-CNP and α-Kv1.1 or α-Kv1.2 followed by simultaneous incubation with 10 μg/ml fluorescein isothiocyanate–conjugated goat anti-rabbit IgG and 10 μg/ml Texas red–conjugated goat anti-mouse IgG (Molecular Probes). Images were collected on a Bio-Rad MRC 600 scanning laser confocal microscope and printed using the Tektronix Phaser II SD dye sublimation system.

Alternatively, sections were examined using a Deltavision SA3 Wide-field Deconvolution microscope (Applied Precision, Inc, Mercer Island, WA) at the Fred Hutchinson Cancer Research Center (Seattle, WA). This system uses fluorescence microscopy, computationally analyzing the Fourier transform of the point spread function to provide a high resolution image (Agard et al., 1989). Using our Nikon 60 × 1.4 NA objective, the minimum resolution measured is 0.117 μm in x and y axes, the z axis being defined by the thickness of the optical sections. At least three 20 μm thick histochemical sections from each of *Tr* sciatic nerve, *shi* spinal cord, *shi* brain stem, and corresponding regions of control C3HeB mouse were serially sectioned using Deltavision optics at 0.2 μm.

RNase Protection Assay

Brains from 9-week-old *shi* (C3HeB-*shi*/*shi*) and wild-type (C3HeB-+/+) mice were dissected prior to homogenization in guanidinium isothiocyanate and RNA isolation. Sequences specific to mKv1.1, mKv1.2, and ribosomal 18S were protected from digestion by RNase A and T1 (Ausubel, 1992). In each assay, RNA loading was monitored by diluting an aliquot of the sample to be assayed by 10^{-4} and protecting a 340 bp fragment of 18S rRNA. This dilution has been shown previously in this laboratory (unpublished data) to be within the linear range of the assay. Gels were analyzed by PhosphorImager (Molecular Dynamics), and the density of protected fragments was quantified at the Fred Hutchinson Cancer Research Center.

In Situ Hybridization

Brains of three young adult (9-week-old) wild-type (C3HeB-+/+) and *shi* (C3HeB-*shi*/*shi*) mice were cut on a cryostat to 20 μm, mounted onto 3-aminopropyltriethoxysilane-treated slides, air dried, processed, hybridized, and washed after hybridization as described (Wang et al., 1994). Slides were dipped in Kodak NTB-2 emulsion (diluted 1:1 in 600 mM NH_4OAC), stored at 4°C for 8 days, developed, and counterstained with hematoxylin blue.

The antisense cRNA probe (riboprobe) for mKv1.1 was transcribed with T7 RNA polymerase from a plasmid that contains 248 bp of mKv1.1 sequence corresponding to 40 bp of 5′ untranslated region and 212 bp from the amino-terminal coding region. The antisense cRNA probe for mKv1.2 was transcribed with T3 RNA polymerase from a plasmid containing 615 bp of 3′ untranslated region and 10 bp of the carboxyl terminus of mKv1.2. The antisense cRNA probe for mKv3.1 is transcribed with T3 RNA polymerase from a plasmid that contains 189 bp of the third exon. These probes correspond to sequences in the nonconserved region among the K^+ channels. Sense riboprobe controls for each riboprobe detected no signals (data not shown).

Image Analysis of Brain Sections after In Situ Hybridization

IOD Reading from Autoradiogram

For each analysis of IOD from corpus callosum, internal capsule, fornix-fimbria, neocortex, hippocampus (CA3), and olfactory bulb (mitral

cell layer), three *shi* and three parental mice were analyzed. Brain sections from *shi* and wild-type mice were paired anatomically (Paxinos and Watson, 1986). Slides from both genotypes were processed simultaneously. Autoradiograms with moderate exposure were chosen for analysis using a MicroComputer Imaging Device (MCID, Imaging Research, Inc., Ontario, Canada). The IOD was calibrated using optical standards. Images of brain sections from autoradiograms were collected using a 50 mm lens with a 36 mm extension tube. The IOD was determined in multiple small circular areas within several anatomically distinct brain regions. Values from the circular sample areas were then averaged to give a measure of channel expression in each region. These values were used to determine a mean ratio between *shi* and wild-type mice for each of the 9 pairs of matched sections. The ratios from 9 pairs of sections were averaged.

Grain/Cell Count

K^+ channel expression was measured on a per cell basis in two brain regions: the corpus callosum and medial and lateral aspects of the deep cerebellar nuclei. Anatomically matched sections from brains of three *shi* and three wild-type mice were analyzed; 3 sections were analyzed in each mouse, giving a total of 9 sections per region per genotype.

Sections were analyzed under light- and dark-field microscopy. The number of grains per cell was estimated by MCID. Labeled cells were identified under light-field microscopy using a 40 × objective and outlined. Silver grains were counted over individual cells.

Acknowledgments

All correspondence should be addressed to B. L T. The authors thank Drs. B. Hille, P. Schwartzkroin, and M. Bosma for comments on the manuscript; L. Robinson for excellent animal care; and P. Goodwin and T. Knight, Fred Hutchinson Cancer Research Center Image Analysis Lab, for their enthusiasm and skill in producing the artwork. This work was supported by grants from the National Institutes of Health (J. L. N. and B. L T.), the Veterans Administration, and the Klingenstein Fund (B. L T.). H. W. was supported by NIH T32-DC00018, Basic Science Training in Otolaryngology.

The cost of publication of this article were defrayed in part by the payment of page charges. This article must therefore be hereby marked *"advertisement"* in accordance with 18 USC Section 1734 solely to indicate this fact.

Received May 25, 1995; revised September 1, 1995.

References

Agard, D.A., Hiraoka, Y., Shaw, P.J., and Sedat, J.W. (1989). Fluorescence microscopy in three dimensions. Meth. Cell Biol. *30*, 353–377.

Ausubel, F.M. (1992). Current Protocols in Molecular Biology (New York: Wiley & Sons), pp. 4.71–4.75.

Baker, M., Bostock, H., Grafe, P., and Martius, P. (1987). Function and distribution of three types of rectifying channel in rat spinal root myelinated axons. J. Physiol. *383*, 45–67.

Barres, B.A. (1991). Glial ion channels. Curr. Opin. Neurobiol. *1*, 354–359.

Bever, C.T.J. (1994). The current status of studies of aminopyridines in patients with multiple sclerosis. Ann. Neurol. *36* (Suppl.), S118–S121.

Bird, T.M., Farrell, D.F., and Sumi, S.M. (1978). Brain lipid composition of the *shiverer* mouse (gene defect in myelin development). J. Neurochem. *31*, 387–391.

Black, J.A., Smith, K.J., Kocsis, J.D., and Waxman, S.G. (1991). Distribution of sodium channels in chronically demyelinated spinal cord axons: immuno-ultrastructural localization and electrophysiological observations. Brain Res. *544*, 59–70.

Bosma, M.M., Allen, M.L., Martin, T.M., and Tempel, B.L (1993). PKA-dependent regulation of mKv1.1, a mouse Shaker-like potassium channel gene, when stably expressed in CHO cells. J. Neurosci. *13*, 5242–5250.

Bostock, H., Sears, T.A., and Sherratt, R.M. (1981). The effects of 4-aminopyridine and tetraethylammonium ions on normal and demyelinated mammalian nerve fibers. J. Physiol. *313*, 301–315.

Bowe, C.M., Kocsis, J.D., and Waxman, S.G. (1985). Differences between mammalian ventral and dorsal spinal roots in response to blockade of potassium channels during maturation. Proc. R. Soc. Lond. (B) *224*, 355–366.

Brismar, T. (1980). Potential clamp analysis of membrane currents in rat myelinated nerve fibers. J. Physiol. *298*, 171–184.

Chiu, S.Y. (1991). Functions and distribution of voltage-gated sodium and potassium channels in mammalian Schwann cells. Glia *4*, 541–558.

Chiu, S.Y., and Ritchie, J.M. (1981). Evidence for the presence of potassium channels in paranodal region of acutely demyelinated mammalian single nerve fibers. J. Physiol. *313*, 415–437.

Chiu, S.Y., and Wilson, G.F. (1989). The role of potassium channels in Schwann cell proliferation in Wallerian degeneration of explant rabbit sciatic nerves. J. Physiol. *408*, 199–222.

Chiu, S.Y., Ritchie, J.M., Rogart, R., and Stagg, D. (1979). A quantitative description of membrane currents in rabbit myelinated nerve. J. Physiol. *292*, 149–166.

Chiu, S.Y., Scherer, S.S., Blonski, M., Kang, S.S., and Messing, A. (1994). Axons regulate the expression of Shaker-like potassium channel genes in Schwann cells in peripheral nerve. Glia *12*, 1–11.

Choi, B.H. (1986). Myelin-forming oligodendrocytes of developing mouse spinal cord: immunocytochemical and ultrastructural studies. J. Neuropath. Exp. Neurol. *45*, 513–524.

Dugandzija-Novakovic, S., Koszowski, A.G., Levinson, S.R., and Shrager, P. (1995). Clustering of Na^+ channels and node of Ranvier formation in remyelinating axons. J. Neurosci. *15*, 492–503.

Gordon, D., Merrick, D., Auld, V., Dunn, R., Goldin, A.L., Davidson, N., and Catterall, W.A. (1987). Tissue-specific expression of the RI and RII sodium channel subtypes. Proc. Natl. Acad. Sci. USA *84*, 8682–8686.

Hille, B. (1992). Ionic Channels of Excitable Membranes, 2nd edition (Sunderland, Massachusetts: Sinauer).

Hopkins, W.F., Allen, M.L., Houamed, K.M., and Tempel, B.L (1994). Properties of voltage-gated K^+ currents expressed in *Xenopus* oocytes by mKv1.1, mKv1.2 and their heteromultimers as revealed by mutagenesis of the dendrotoxin binding site in mKv1.1. Pflügers Arch. *428*, 382–390.

Mi, H., Deerinck, T.J., Ellisman, M.H., and Schwarz, T.L. (1995). Differential distribution of closely related potassium channels in rat Schwann cells. J. Neurosci. *15*, 3761–3774.

Molineaux, S.M., Engh, H., deFerra, F., Hudson, L., and Lazzarini, R.A. (1986). Recombination within the myelin basic protein gene created the dysmyelinating *shiverer* mouse mutation. Proc. Natl. Acad. Sci. USA *83*, 7542–7546.

Moll, C., Mourre, C., Lazdunski, M., and Ulrich, J. (1991). Increase of sodium channels in demyelinated lesions of multiple sclerosis. Brain Res. *556*, 311–316.

Noebels, J.L., Marcom, P.K., and Jalilian-Tehrani, M.H. (1991). Sodium channel density in hypomyelinated brain increased by myelin basic protein gene deletion. Nature *352*, 431–433.

Paxinos, G., and Watson, C. (1986). The Rat Brain in Stereotaxic Coordinates (Orlando, Florida: Academic Press).

Privat, A., Jacque, C., Bourre, J.M., Dupouey, P., and Baumann, N. (1979). Absence of the major dense line in myelin of mutant mouse "*shiverer*." Neurosci. Lett. *12*, 107–112.

Roach, A., Takahashi, N., Pravtcheva, D., Ruddle, F., and Hood, L. (1985). Chromosomal mapping of mouse myelin basic protein gene and structure and transcription of the partially deleted gene in *shiverer* mutant mice. Cell *42*, 149–155.

Röper, J., and Schwarz, J.R. (1989). Heterogenous distribution of fast and slow potassium channels in myelinated rat nerve fibers. J. Physiol. *416*, 93–110.

Rosenbluth, J. (1980a). Peripheral myelin in the mouse mutant *shiverer*. J. Comp. Neurol. *193*, 729–740.

Rosenbluth, J. (1980b). Central myelin in the mouse mutant *shiverer*. J. Comp. Neurol. *194*, 639–648.

Rosenbluth, J. (1981). Axoglial junctions in the mouse mutant *shiverer*. Brain Res. *208*, 283–297.

Rosenbluth, J. (1988). Role of glial cells in differentiation and function of myelinated axons. Int. J. Dev. Neurosci. *6*, 3–24.

Scheinman, R.I., Auld, V.J., Goldin, A.L., Davidson, N., Dunn, R.J., and Catterall, W.A. (1989). Developmental regulation of sodium channel expression in the rat forebrain. J. Biol. Chem. *264*, 10660–10666.

Schwarz, J.R., Corrette, B.J., Mann, K., and Wietholter, H. (1991). Changes of ionic channel distribution in myelinated nerve fibers from rats with experimental allergic neuritis. Neurosci. Lett. *122*, 205–209.

Shrager, P. (1989). Sodium channels in single demyelinated mammalian axons. Brain Res. *483*, 149–154.

Sprinkle, T.J. (1989). 2′,3′-Cyclic nucleotide 3′-phosphodiesterase, an oligodendrocyte-Schwann cell and myelin-associated enzyme of the nervous system. CRC Crit. Rev. Neurobiol. *4*, 235–301.

Stefoski, D., Davis, F.A., Faut, M., and Schauf, C.L. (1987). 4-Aminopyridine improves clinical signs in multiple sclerosis. Ann. Neurol. *21*, 71–77.

Sternberger, L.A. (1979). Immunocytochemistry (New York: Wiley).

Suter, U., Welcher, A.A., Ozcelik, T., Snipes, G.J., Kosaras, B., Francke, U., Billing-Gagliardi, S., Sidman, R.L., and Shooter, E.M. (1992). *Trembler* mouse carries a point mutation in a myelin gene. Nature *356*, 241–244.

Targ, E.F., and Kocsis, J.D. (1985). 4-Aminopyridine leads to restoration of conduction in demyelinated rat sciatic nerve. Brain Res. *328*, 358–361.

Valentijn, L.J., Baas, F., Wolterman, R.A., Hoogendijk, J.E., van den Bosch, N.H., Zorn, I., Gabreels-Festen, A.W., de Visser, M., and Bolhuis, P.A. (1992). Identical point mutations of PMP-22 in *Trembler*^{J} mouse and Charcot-Marie-Tooth disease type 1A. Nature Genet. *2*, 288–291.

Wang, H., Kunkel, D.D., Martin, T.M., Schwartzkroin, P.A., and Tempel, B.L (1993). Heteromultimeric K^+ channels in terminal and juxtaparanodal regions of neurons. Nature *365*, 75–79.

Wang, H., Kunkel, D.D., Schwartzkrion, P.A., and Tempel, B.L (1994). Localization of Kv1.1 and Kv1.2, two K channel proteins, to synaptic terminals, somata and dendrites in the mouse brain. J. Neurosci. *14*, 4588–4599.

Waxman, S.G., and Ritchie, J.M. (1985). Organization of ion channels in the myelinated nerve fiber. Science *228*, 1502–1507.

Waxman, S.G., and Wood, S.L. (1984). Impulse conduction in inhomogenous axons: effects of variation in voltage-sensitive ionic conductances on invasion of demyelinated axon segments of preterminal fibers. Brain Res. *294*, 111–122.

Werkman, T.R., Kawamura, T., Yokoyama, S.H.H., and Rogowski, M.A. (1992). Charybdotoxin, dendrotoxin and mast cell degranulating peptide block the voltage-activated K^+ current of fibroblast cells stable transfected with NGK1 (Kv1.2) K^+ channel complementary DNA. Neuroscience *50*, 935–946.

Westenbroek, R.E., Noebels, J.L., and Catterall, W.A. (1992). Elevated expression of Type II Na^+ channels in hypomyelinated axons of *shiverer* mouse brain. J. Neurosci. *12*, 2259–2267.

Wiley-Livigston, C., and Ellisman, M.H. (1980). Development of axonal membrane specializations defines nodes of Ranvier and precedes Schwann cell myelin elaboration. Dev. Biol. *79*, 334–355.

Wilson, G.F., and Chiu, S.Y. (1990). Ion channels in axon and Schwann cell membranes at paranodes of mammalian myelinated fibers studied with patch-clamp. J. Neurosci. *10*, 3263–3274.